Composites Communications 24 (2021) 100677

Contents lists available at ScienceDirect

Composites Communications

journal homepage: www.elsevier.com/locate/coco

Stretchable and self-healing polyvinyl alcohol/cellulose nanofiber nanocomposite hydrogels for strain sensors with high sensitivity and linearity

Kaiwen Xu [a], Yufeng Wang [a], Bing Zhang [a], Chao Zhang [a,*], Tianxi Liu [a,b]

[a] State Key Laboratory for Modification of Chemical Fibers and Polymer Materials, College of Materials Science and Engineering, Innovation Center for Textile Science and Technology, Donghua University, Shanghai, 201620, PR China

[b] Key Laboratory of Synthetic and Biological Colloids, Ministry of Education, School of Chemical and Material Engineering, Jiangnan University, Wuxi, 214122, PR China

ARTICLE INFO

Keywords:
Nanocomposite hydrogel
Cellulose nanofiber
Self-healing performance
Strain sensors

ABSTRACT

The development of wearable strain sensors with high sensitivity, linearity and self-healing property is highly demanded. Herein, a simple yet efficient solution compounding method is proposed for fabricating a cellulose nanofiber reinforced borax/polyvinyl alcohol nanocomposite hydrogel (CBPH). The resultant CBPH exhibited largely enhanced ultimate tensile strength (47.1 kPa) and high toughness (213.9 kJ m^{-3}) compared with that of neat borax/polyvinyl alcohol hydrogel (3.4 kPa, 44.3 kJ m^{-3}), ascribing to efficient load transfer between dynamically hydrogen-bonded cellulose nanofiber and polyvinyl alcohol. Besides, dynamic borate-diol bonds among the CBPH contributed to self-healing performance with a healing efficiency reaching nearly 60%. Due to its large stretchability, high toughness and favorable ionic conductivity, the CBPH was used as a stretchable and self-healing ionic conductor for assembling a wearable strain sensor, showing a high yet linear sensitivity (~1.86) over a wide strain range of 0–100%, fast response time (<240 ms) and stable signal feedbacks for human motion detection.

1. Introduction

With the prosperity and development of flexible electronics technology, flexible sensing devices have attracted extensive attention [1,2]. Sensing materials in such devices are required to be capable of quickly converting external stimuli (e.g., temperature [3–6], strain [2,7,8] or pressure [9,10]) into detectable electronic signals. Human skin is regarded as an excellent sample for the development of flexible sensing materials [11–14], which is a natural sensor and inherently equipped with good stretchability, high toughness and self-healing ability. It is quite essential to develop an advanced skin-like sensing material for health monitoring and human-machine interfaces in the era of the Internet of Things [15].

Hydrogels are physically or chemically cross-linked hydrophilic polymer networks that are swollen in an aqueous medium [16]. Due to the water-rich nature and three-dimensional network structure, a myriad of hydrogels possess good biocompatibility and stretchability [17,18], showing great prospects in the fields of wearable devices [19–21], artificial intelligence [22] and soft robotics [23,24]. Besides, considering the complex surface conditions that would occur in many application scenarios, good mechanical adaptability enables sensors to make well contact to irregular interfaces to deliver accurate signals, which is therefore an advantage of many soft hydrogels [25]. Ions can be brought into hydrogels to realize high ionic conductivity by incorporating salts or ionic pendant groups [26–28]. Ionic conductive hydrogels can not only be intrinsically stretchable but also guarantee stable conductivity responses during the deformation [11,29]. Therefore, ionic conductive hydrogels have more similarities to human skin both in mechanical property and transmission mechanism of signals, having great potentials in bionic sensing applications.

Polyvinyl alcohol (PVA)-based hydrogels are prospective alternatives as flexible sensing materials [30]. PVA is noted for many advantages, such as biodegradability, nontoxicity, and biocompatibility [31]. More importantly, the abundant hydroxyl groups on PVA chains bring about a great possibility of developing PVA hydrogels with physical or chemical cross-linking. Borate-diol bonds in hydrogels have been proven

* Corresponding author.
E-mail address: czhang@dhu.edu.cn (C. Zhang).

https://doi.org/10.1016/j.coco.2021.100677
Received 14 January 2021; Received in revised form 9 February 2021; Accepted 9 February 2021
Available online 21 February 2021

to have rapid self-healing properties [32–34]. However, the healing process requires high mobility of PVA chains, which indicates that hydrogels with such self-healing properties might be accompanied by limited mechanical strength and poor shape stability [20,35]. Whereas, it is mechanical properties that significantly influence the signal reliability and sensitivity of sensors based on hydrogels [36]. To keep a balance between mechanical properties and self-healing property, it is a good choice to incorporate certain components for the formation of nanocomposites to provide additional noncovalent interactions, which might promote the healed hydrogels to restore most of their original performance [30,37]. Cellulose nanofibers (CNF), a kind of biodegradable polysaccharide in nanoscale, are characterized by a spatial network structure formed by the physical entanglement of nanofibers [38]. Adequate sodium carboxylate groups (−COO–Na^+) on the CNF are capable of not only realizing good dispersibility in aqueous solution, but also introducing more noncovalent interactions with the hydrogel matrix [32,39]. Moreover, the numerous –COO^-Na^+ from CNF contribute more ions, which can further enhance the ionic conductivity of hydrogels.

Herein, a simple yet efficient solution-compounding method is proposed for fabricating a CNF reinforced borax/PVA nanocomposite hydrogel (CBPH) with excellent mechanical performance, good shape stability and self-healing ability. Among the CBPH, a borax/PVA hydrogel as a self-healable matrix was achieved due to the formation of dynamic borate-diol bonds between PVA and hydrolysate of borax, while physical entanglements and hydrogen-bonded interactions between CNF and PVA hydrogel matrix significantly promoted mechanical properties of the PVA matrix. The as-prepared CBPH was assembled into a resistance-type strain sensor, exhibiting high sensitivity, linearity, and stable signal feedbacks for detecting human motion.

2. Results and discussion

A schematic of the network structures among the CBPH is shown in Fig. 1. There existed two types of networks among the CBPH. First is the dynamic borate-diol bonds between PVA and hydrolysate of borax ($B(OH)_4^-$) [40], and second is the physical entanglements and hydrogen bonds among the CNF and PVA hydrogel matrix (Fig. S1). The dynamic borate-diol bonds among the CBPH contributed to a dynamic restructuring and self-healing process after being damaged. The CNF not only had mechanical reinforcing effects as typical nanofillers, but also provided additional physical entanglements and noncovalent interactions with PVA chains for regulating rheological behaviors of CBPH. The borax/PVA hydrogel (BPH) showed an excellent self-healing ability accompanied by low mechanical strength, and obvious creep deformation of BPH was observed in 60 min (Fig. S2a). However, the shape stability of the resultant CBPH was much higher than that of BPH (Fig. S2b, c), indicating that the addition of CNT reduced the mobility of PVA chains. Tensile tests of BPH with different borax contents were used to explore the effects of borax on the mechanical properties of hydrogels. Although the tensile strength and modulus were enhanced with an increased amount of borax, high crosslinking density greatly decreased the ductility of BPH as the borax content reached 2.0% (Fig. S3). Therefore, the BPH with the borax content of 1.0% was chosen as the matrix for the subsequent fabrication of CBPH. Here, the CBPH was marked as CBPH-X, where X represented the percentage contents of CNF within the CBPH that varied from 0.1 to 1.0 wt%.

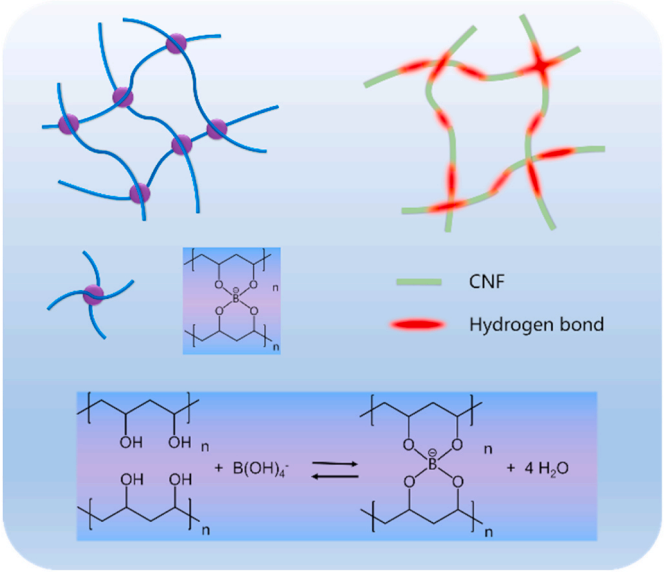

Fig. 1. Schematic diagram of the CBPH with the dynamic borate-diol bonds and hydrogen-bonded CNF network.

The interactions between the PVA, borax, and CNF within the CBPH were explored by infrared spectroscopy (Fig. S4). The peak at 3318 cm^{-1} in the BPH belonged to the stretching vibration of –OH groups, and the corresponding peak of CBPH appeared at 3311 cm^{-1}. The shift of the absorption indicated that the addition of CNF enhanced the hydrogen bonding in the CBPH [41]. Moreover, the strong C═O stretching band in the spectrum of CNF, belonging to –COO^-, was located at 1592 cm^{-1}, which was lower than that in the CBPH (1604 cm^{-1}). This further proved the existence of hydrogen bonding among the CBPH. Besides, the asymmetric stretching relaxation of B–*O*–C at 1417 and 1338 cm^{-1} indicated the presence of interactions between the PVA and borate [35].

Uniaxial tensile tests were further performed to quantify the mechanical properties of CBPH (Fig. 2a). Detailed mechanical properties were summarized in Table 1, and the elastic moduli and fracture energies of BPH and CBPHs were visually presented in Fig. 2b. Both the ultimate stress and elastic modulus showed monotonic increases with an increasing amount of CNF. The ultimate stress of CBPH gradually increased to 8.8, 19.7, 47.4 and 58.1 kPa with an increasing CNF content of 0.1, 0.2, 0.5 and 1.0 wt%, respectively, suggesting that the addition of CNF resulted in gradual increases in mechanical strength and rigidity of CBPH. The ultimate stress of CBPH-1.0 was about 16 times that for BPH (3.4 kPa) with a decreased elongation at break of 289.1%, only 22.4% of the elongation at break for the BPH (1289.1%). Meanwhile, the CBPH-0.1, CBPH-0.2 and CBPH-0.5 also showed decreases in the elongation at break with similar characteristics, because the destruction of the strongly entangled CNF network led to the failure in maintaining the integrality of CBPH at a high strain. The fracture energy reflected the toughness of BPH and CBPHs. Despite a large fracture strain, the limited ultimate strength of BPH accounted for low fracture energy of 44.3 kJ m^{-3}. In contrast, the CBPHs showed significant increases in toughness. An obvious rise in tensile strength appeared when the CNF content increased to 0.5%, and the fracture energy reached 213.9 kJ m^{-3}, indicating that the addition of CNF effectively enhanced load transfer and energy dissipation of the applied stress. Such increments in elastic modulus and toughness are attributed to the physical entanglements and extra hydrogen-bonded interactions provided by the CNF. However, as the amount of CNF further increased to 1.0 wt%, the fracture energy and elongation at break sharply decreased to 142.4 kJ m^{-3} and 290%, respectively, indicating that excessive CNF led to a fragile CBPH. The cyclic tensile test of CBPH-0.5 was conducted at a 50% strain for 100 cycles. The large hysteresis at the beginning of tensile cycles was mainly ascribed to the rearrangement of CNF, PVA chains and dynamic bonds among the CBPH. The subsequent curves showed a relatively stable trend and almost overlapped after 25 cycles, indicating the good fatigue resistance of CBPH-0.5 (Fig. S5).

The presence of CNF directly caused significant changes in the viscoelastic characteristics of BPH ascribing to the formation of physical entanglements and hydrogen-bonded interactions between the CNF and PVA hydrogel matrix. The viscoelasticity of CBPHs was further characterized by rheological measurements to investigate the effects of the

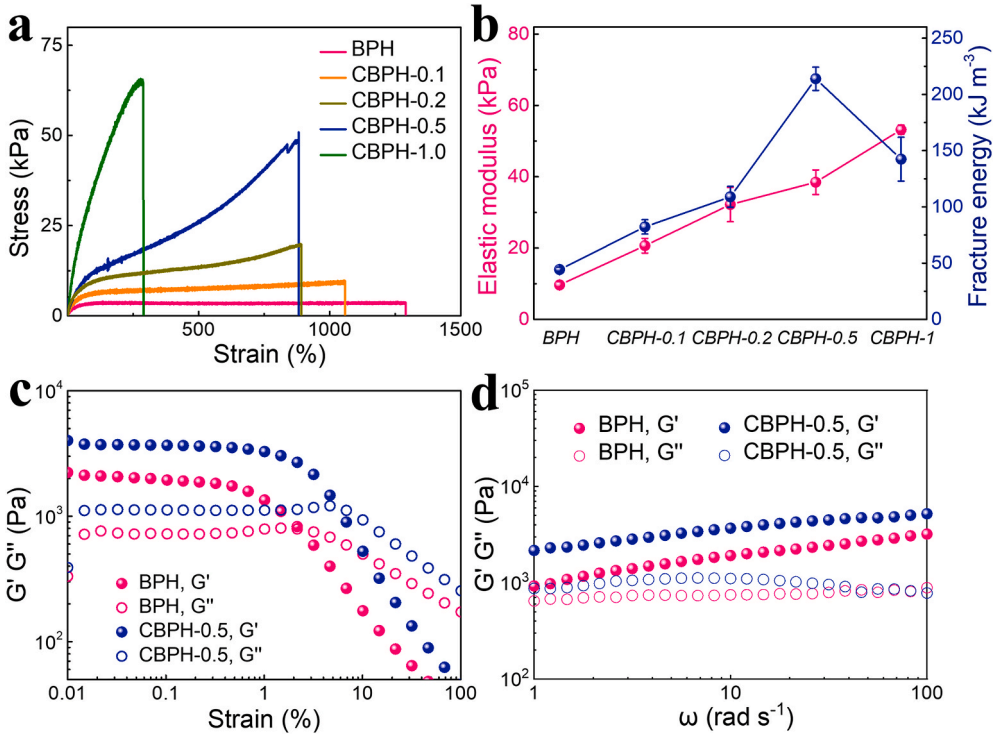

Fig. 2. (a) Typical stress-strain curves of BPH and its nanocomposite hydrogels. (b) Elastic modulus and fracture energy of BPH and its nanocomposite hydrogels. Rheological properties of BPH and CBPH-0.5 at 25 °C: (c) Strain sweep at a fixed frequency of 10 rad s^{-1}; (d) Oscillatory frequency sweep at a fixed shear strain of 0.1%.

Table 1
Summary of mechanical performance of BPH and its nanocomposite hydrogels.

Samples	Elastic modulus (kPa)	Ultimate strength (kPa)	Elongation at break (%)	Toughness (kJ m^{-3})
BPH	9.6 ± 0.9	3.4 ± 0.1	1289.1 ± 53.3	44.3 ± 2.1
CBPH-0.1	20.7 ± 2.1	8.8 ± 1.2	1060.1 ± 27.7	82.2 ± 6.3
CBPH-0.2	32.2 ± 4.8	19.7 ± 3.8	904.9 ± 12.1	108.9 ± 9.3
CBPH-0.5	38.5 ± 3.4	47.4 ± 4.2	879.8 ± 8.9	213.9 ± 10.3
CBPH-1.0	53.2 ± 1.3	58.1 ± 9.3	289.1 ± 8.8	142.4 ± 19.5

addition of CNF within the CBPH. In strain sweep tests, the storage modulus (G′) and loss modulus (G″) was enhanced with increasing contents of CNF, indicating that the introduction of CNF enhanced the rigidity of CBPH (Fig. 2c, S6a). As the shear strain increased, the values of G′ and G″ decreased at a certain strain and an intersection point appeared. The G′ value was larger than that of G″ before this point, indicating that the CBPH exhibited an elastic behavior at an ambient condition, while the gel network was unstable after this point. When the intersection point occurred at a higher strain, it meant that the network of CBPH showed stronger resistance to deformation with higher toughness [42]. The intersection point of CBPH-0.5 appeared at a strain of 5.6%, indicating that the CBPH-0.5 had an optimized resistance to deformation and toughness among the CBPH. Oscillatory frequency sweep was carried out in the linear viscoelastic region obtained in the strain sweep of BPH and CBPHs (Fig. 2d, S6b), indicating that the BPH and CBPH did not exhibit stable cross-linking network characteristics. In contrast, the G′ values of BPH and CBPHs showed a monotonous increase with an increase in the shearing frequency, while the G″ values of CBPHs decreased in the high-frequency region. Therefore, the CBPH showed strong frequency-dependent and obvious elastic characteristics at high frequency. The intersection point between the curves of G′ and G″ in the frequency sweep was a sign of gelation, indicating that an elastic gel was formed by chain entanglements and reversible cross-linking. According to the trend of G′ and G″ values, the intersection point of CBPH-0.5 occurred at a lower frequency than that of BPH. This indicated that the CBPH-0.5 exhibited tolerance to deformation under low-frequency shear strain, i.e., good shape stability. Regarding the significance of mechanical strength, toughness and shape stability of hydrogels for flexible sensing devices, the CBPH-0.5 was selected as an optimized sample for subsequent characterizations.

The CBPH-0.5 is also equipped with self-healing property inherited from the BPH matrix. The CBPH-0.5 acting as an ionic conductor was connected to a circuit to successfully lighten up an LED. After being cut apart, the CBPH-0.5 was capable of self-healing by contacting with each other and restoring its ionic conductivity (Fig. 3a). Fig. 3b exhibits optical micrographs during the cutting/healing processes of CBPH-0.5 with various healing time. Due to the self-healing of the incision, the originally clear notch gradually became blurred. After a healing process for 12 h, the notch of the CBPH-0.5 self-healed completely. Besides, the self-healing behavior of the CBPH-0.5 was further studied by continuous step oscillation measurements (Fig. 3c). When the CBPH-0.5 was subjected to a 50% strain, the G′ value sharply decreased and the G″ value increased, indicating the collapse of the dynamic network. After a sudden change to 1% strain, the G′ immediately recovered to ~60% of its original value, and then recovered to ~90% within 30 s. The breakage and recovery behaviors were continually repeated several times, indicating that the elastic network of CPBH-0.5 quickly reconstructed, further verifying its good self-healing property. To evaluate the healing efficiency of mechanical properties of CBPH-0.5, tensile testing was performed for CBPHs-0.5 under various healing time (Fig. 3d). The healing efficiency was calculated according to the recovery of fracture energy, relative to that of the representative CBPH-0.5 (Fig. 3e). The healing efficiency was ~19.4% after a 1 h healing process, and the healing efficiencies reached 43.2% and 58.5% after healing for 12 and 24 h, respectively. The CBPH-0.5 presented a time-dependent healing characteristic, similar to the

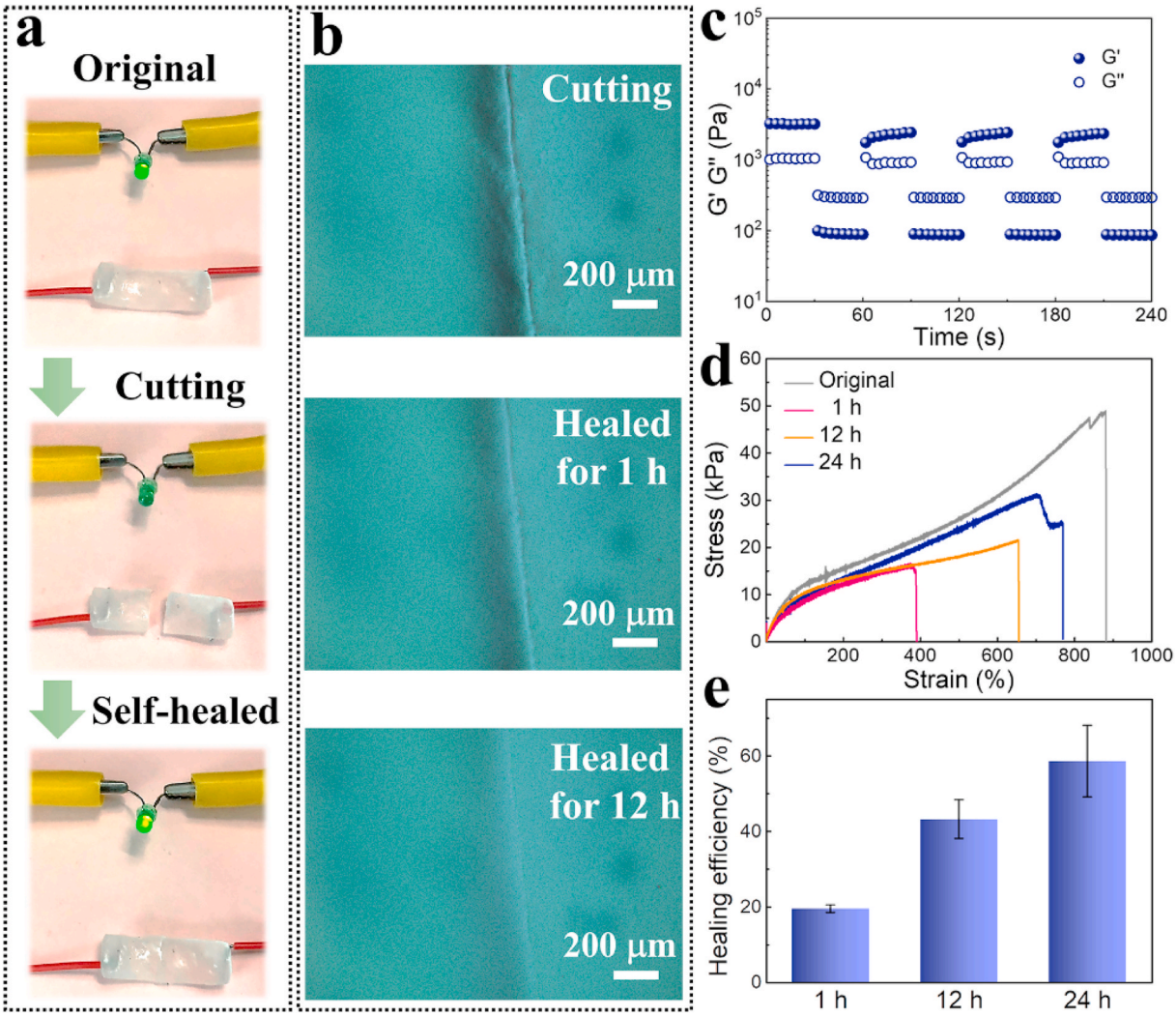

Fig. 3. Self-healing performance of the CBPH-0.5. (a) Photographs showing the recovery of ionic conductivity of CBPH-0.5 during the cutting and self-healing process. (b) Optical micrographs of the cracked CBPH-0.5 during the cutting and self-healing processes. (c) Continuous step oscillation measurements from 1% to 50% and back to 1% strain at 10 rad s^{-1} for every 30 s. (d) Representative stress-strain curves of the initial and self-healed CBPH-0.5 under various healing time. (e) Healing efficiency of the CBPH-0.5 under various healing time.

human skin. Once the original entanglement network of CNF was broken, it took a long time to restore a strong network via dynamic interactions. Moreover, the uniform distribution of CNF in the PVA matrix might hinder the mobility of PVA chains and reduce the probability of the formation of borate-diol bonds.

Borate and sodium ions derived from the borax and CNF accounted for the high ionic conductivity of CBPH. The ionic conductivities of BPH, CBPH, and healed CBPH were measured. The ionic conductivity of CBPH was as high as 0.73 S m^{-1}, and the ionic conductivity of healed CBPH reached 0.71 S m^{-1} (Fig. S7), suggesting an excellent recovery of ionic conductivity upon cutting and self-healing. The CBPH-0.5 was assembled into a resistance-type strain sensor, encapsulated by VHB tapes to prevent dehydrations (Fig. 4a). The resistance changes caused by various strain changes and human movements were monitored in real-time. Fig. 4b displays the relationship between the resistance variations and tensile strains during stretching/recovery processes. The curves showed high linearity and are consistent for various cycles. The CBPH-0.5 strain sensor exhibited high sensitivity (~1.86) according to linear fitting. The stepped stretching and recovery processes were employed to verify the reliability of sensing signals (Fig. 4c). The resistance variations showed corresponding trends with the applied strain that was controlled by the preset program. The resistance variations remained repeatable and stable at the corresponding strains during the stretching/recovery process. Furthermore, a 50% strain was rapidly applied (~120 ms) to verify the instant response characteristic of the sensor (Fig. 4d). Fig. 4e is an enlarged view of the resistance changing trend of the rapid quantitative stretching process, and the response time was ~240 ms. The CBPH-0.5 sensor also showed an instant response (~244 ms) in the recovery process (Fig. S8). The stability of sensors composed of original and healed CBPH-0.5 was further evaluated through cyclic stretching tests. Both the sensors underwent cyclic stretching to a 100% strain. The healed CBPH-0.5 was self-healed for 24 h before testing, and the resistance variations were almost consistent with that of CBPH-0.5 in its original state (Fig. 4f). The resistance variations of both the original and healed CBPH-0.5 exhibited good repeatability and little drift, confirming the high stability and recovery of the resistance responses. Therefore, the CBPH-0.5 sensor could effectively distinguish the magnitude of the applied strains according to the changes of the resistance signals during the process of tensile deformation. It also could realize functional recovery through the self-healing process after an accidental failure, indicating great potentials for monitoring complex strain conditions. To verify the motion perception ability of the CBPH-0.5 sensor, it was directly attached to different parts of the human body. The resistance variations showed a

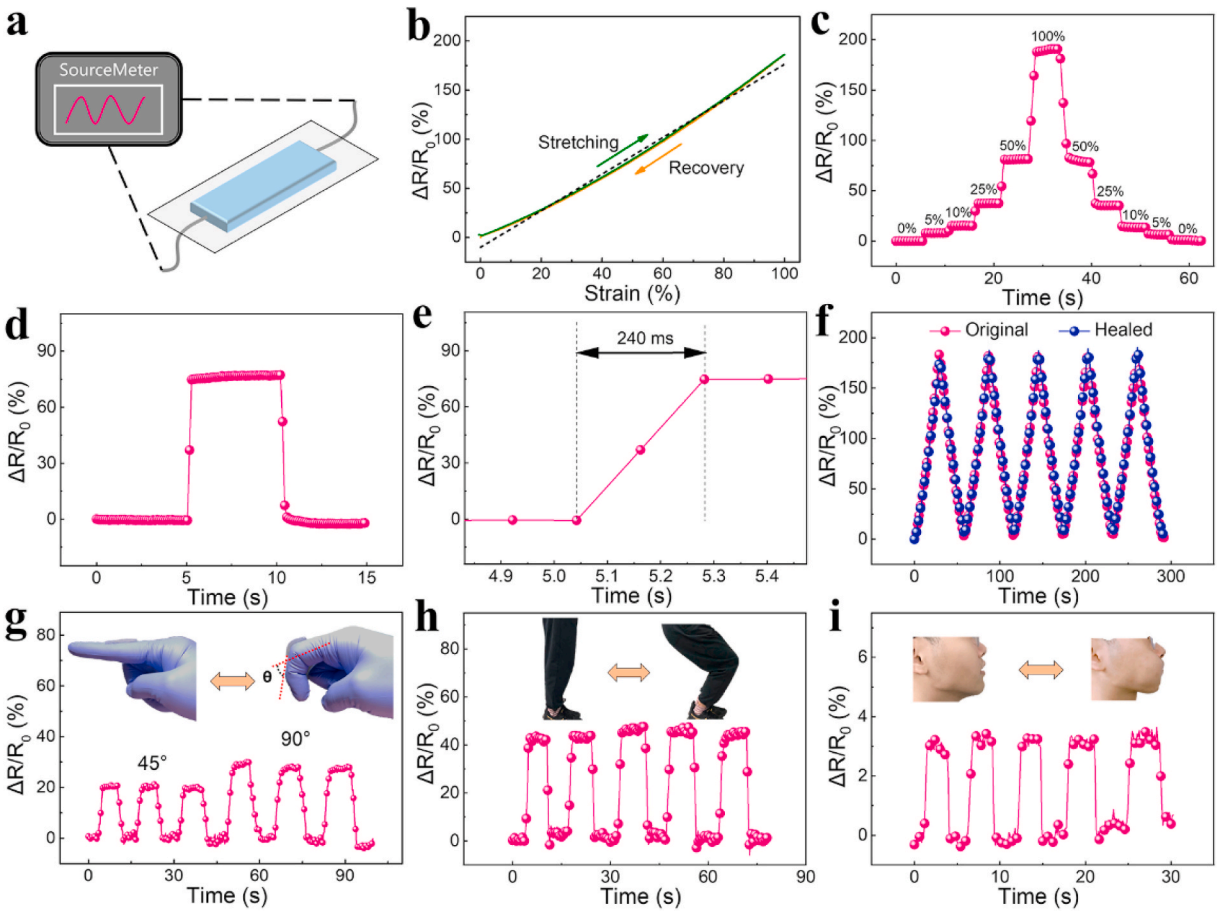

Fig. 4. Sensing performance of strain sensors based on the CBPH-0.5. (a) Schematic diagram showing the assembly of CBPH-0.5 into a strain sensor, where one piece of CBPH-0.5 was encapsulated between 3 M VHB tapes with Cu wires at both ends. (b) Resistance variations during stretching and recovery. (c) Resistance variations and signal stability at different strains. (d) Instant response to a strain of 50%. (e) Enlarged view of the rapid stretching in (d). (f) Resistance variations before and after cutting and self-healing under continuous cyclic tests. Strain sensors monitoring human motions including (g) finger bending, (h) knee flexion, and (i) facial muscle movement. Insets in (g–i) are photographs of the corresponding motions.

good response to finger bending at different angles (45°, 90°) (Fig. 4g), knee flexion during the squat (Fig. 4h), and movements of facial muscles caused by inflating in the mouth (Fig. 4i). The CBPH-0.5 sensor exhibited excellent resistance-type sensing performance, indicating its great potentials in sensing applications for artificial intelligence, human-machine interfaces, and wearable devices.

3. Conclusion

In summary, a highly stretchable and self-healable nanocomposite hydrogel (CBPH) was fabricated by a solution-processed compounding of PVA, borax and CNF. Dynamic borate-diol bonds between PVA and hydrolysate of borax were achieved among the CBPH, contributing to its self-healing performance at room temperature. Hydrogen-bonded interactions between CNF and PVA were beneficial to mechanical strengthening and toughening of the PVA hydrogel matrix. Among the CBPH with various CNF loadings, the CBPH-0.5 exhibited enhanced mechanical strength (47.4 kPa), high toughness (213.9 kJ m^{-3}), large elongation at break (880%) and self-healing performance with a healing efficiency of 58.5%. The as-prepared ionic conductive CBPH-0.5 was directly assembled into a resistance-type strain sensor, showing high and linear sensitivity (~1.86) within a strain range of 0–100%, instant resistive response (<240 ms), and stable signal feedbacks for human motion detection. The development of ionic conductive CBPH might provide a competitive alternative for the next-generation self-healable ionic conductors and wearable strain sensing devices.

CRediT authorship contribution statement

Kaiwen Xu: Visualization, Investigation, Data curation, Writing – original draft. **Yufeng Wang:** Visualization, Investigation, Writing – review & editing. **Bing Zhang:** Investigation, Writing – review & editing. **Chao Zhang:** Conceptualization, Methodology, Supervision, Writing – review & editing. **Tianxi Liu:** Conceptualization, Supervision.

Declaration of competing interest

The authors declare that they have no known competing financial interests or personal relationships that could have appeared to influence the work reported in this paper.

Acknowledgements

We are grateful for the financial support from the National Natural Science Foundation of China (21875033), the Shanghai Rising-Star Program (18QA1400200), the Shanghai Scientific and Technological Innovation Project (18JC1410600), and Ministry of Education of the People's Republic of China (6141A02033233).

References

[1] M. Amjadi, K.-U. Kyung, I. Park, M. Sitti, Stretchable, skin-mountable, and wearable strain sensors and their potential applications: a review, Adv. Funct. Mater. 26 (2016) 1678–1698.

[2] S. Wu, S. Peng, Y. Yu, C.H. Wang, Strategies for designing stretchable strain sensors and conductors, Adv. Mater. Technol. 5 (2020) 1900908.
[3] Z. Wang, H. Zhou, W. Chen, Q. Li, B. Yan, X. Jin, A. Ma, H. Liu, W. Zhao, Dually synergetic network hydrogels with integrated mechanical stretchability, thermal responsiveness, and electrical conductivity for strain sensors and temperature alertors, ACS Appl. Mater. Interfaces 10 (2018) 14045–14054.
[4] G. Liu, Q. Tan, H. Kou, L. Zhang, J. Wang, W. Lv, H. Dong, J. Xiong, A flexible temperature sensor based on reduced graphene oxide for robot skin used in Internet of Things, Sensors 18 (2018) 1400.
[5] S. Nakata, T. Arie, S. Akita, K. Takei, Wearable, flexible, and multifunctional healthcare device with an ISFET chemical sensor for simultaneous sweat pH and skin temperature monitoring, ACS Sens. 2 (2017) 443–448.
[6] W. Du, J. Zhang, Z. Zhao, X. Zhang, Preparation of novel temperature-responsive double-network hydrogel reinforced with aramid nanofibers, Compos. Commun. 22 (2020) 100438.
[7] C.M. Boutry, Y. Kaizawa, B.C. Schroeder, A. Chortos, A. Legrand, Z. Wang, J. Chang, P. Fox, Z. Bao, A stretchable and biodegradable strain and pressure sensor for orthopaedic application, Nat. Electron. 1 (2018) 314–321.
[8] C. Tan, Z. Dong, Y. Li, H. Zhao, X. Huang, Z. Zhou, J.-W. Jiang, Y.-Z. Long, P. Jiang, T.-Y. Zhang, B. Sun, A high performance wearable strain sensor with advanced thermal management for motion monitoring, Nat. Commun. 11 (2020) 3530.
[9] S. Lee, A. Reuveny, J. Reeder, S. Lee, H. Jin, Q. Liu, T. Yokota, T. Sekitani, T. Isoyama, Y. Abe, Z. Suo, T. Someya, A transparent bending-insensitive pressure sensor, Nat. Nanotechnol. 11 (2016) 472–478.
[10] C. Wang, D. Hwang, Z. Yu, K. Takei, J. Park, T. Chen, B. Ma, A. Javey, User-interactive electronic skin for instantaneous pressure visualization, Nat. Mater. 12 (2013) 899–904.
[11] J.-Y. Sun, C. Keplinger, G.M. Whitesides, Z. Suo, Ionic skin, Adv. Mater. 26 (2014) 7608–7614.
[12] Y. Song, H. Chen, Z. Su, X. Chen, L. Miao, J. Zhang, X. Cheng, H. Zhang, Highly compressible integrated supercapacitor–piezoresistance-sensor system with CNT–PDMS sponge for health monitoring, Small 13 (2017) 1702091.
[13] Z. Lei, J. Huang, P. Wu, Traditional dough in the era of Internet of Things: edible, renewable, and reconfigurable skin-like iontronics, Adv. Funct. Mater. 30 (2019) 1908018.
[14] K. Xu, Y. Lu, K. Takei, Multifunctional skin-inspired flexible sensor systems for wearable electronics, Adv. Mater. Technol. 4 (2019) 1800628.
[15] Y. Yang, G. Chiesura, B. Plovie, T. Vervust, G. Luyckx, J. Degrieck, T. Sekitani, J. Vanfleteren, Design and integration of flexible sensor matrix for in situ monitoring of polymer composites, ACS Sens. 3 (2018) 1698–1705.
[16] Y.S. Zhang, A. Khademhosseini, Advances in engineering hydrogels, Science 356 (2017), eaaf3627.
[17] J.H. Lee, H.W. Kim, Emerging properties of hydrogels in tissue engineering, J. Tissue Eng. 9 (2018), 2041731418768285.
[18] J.-j. Duan, L.-n. Zhang, Robust and smart hydrogels based on natural polymers, Chin. J. Polym. Sci. 35 (2017) 1165–1180.
[19] T. Li, Y. Li, T. Zhang, Materials, structures, and functions for flexible and stretchable biomimetic Sensors, Acc. Chem. Res. 52 (2019) 288–296.
[20] X. Jing, H. Li, H.-Y. Mi, Y.-J. Liu, P.-Y. Feng, Y.-M. Tan, L.-S. Turng, Highly transparent, stretchable, and rapid self-healing polyvinyl alcohol/cellulose nanofibril hydrogel sensors for sensitive pressure sensing and human motion detection, Sens. Actuators, B 295 (2019) 159–167.
[21] J. Mao, C. Zhao, Y. Li, D. Xiang, Z. Wang, Highly stretchable, self-healing, and strain-sensitive based on double-crosslinked nanocomposite hydrogel, Compos. Commun. 17 (2020) 22–27.
[22] X. Wang, L. Dong, H. Zhang, R. Yu, C. Pan, Z.L. Wang, Recent progress in electronic skin, Adv. Sci. 2 (2015) 1500169.
[23] S. Bauer, S. Bauer-Gogonea, I. Graz, M. Kaltenbrunner, C. Keplinger, R. Schwödiauer, 25th anniversary article: a soft future: from robots and sensor skin to energy Harvesters, Adv. Mater. 26 (2014) 149–162.
[24] H. Yuk, S. Lin, C. Ma, M. Takaffoli, N.X. Fang, X. Zhao, Hydraulic hydrogel actuators and robots optically and sonically camouflaged in water, Nat. Commun. 8 (2017) 14230.
[25] Z. Lei, Q. Wang, S. Sun, W. Zhu, P. Wu, A bioinspired mineral hydrogel as a self-healable, mechanically adaptable ionic skin for highly sensitive pressure sensing, Adv. Mater. 29 (2017) 1700321.
[26] Z. Wang, Y. Cong, J. Fu, Stretchable and tough conductive hydrogels for flexible pressure and strain sensors, J. Mater. Chem. B 8 (2020) 3437–3459.
[27] Z. Liu, Y. Wang, Y. Ren, G. Jin, C. Zhang, W. Chen, F. Yan, Poly(ionic liquid) hydrogel-based anti-freezing ionic skin for a soft robotic gripper, Mater. Horiz. 7 (2020) 919–927.
[28] C. Yang, Z. Suo, Hydrogel ionotronics, Nat. Rev. Mater. 3 (2018) 125–142.
[29] Y. Ye, Y. Zhang, Y. Chen, X. Han, F. Jiang, Cellulose nanofibrils enhanced, strong, stretchable, freezing-tolerant ionic conductive organohydrogel for multi-functional sensors, Adv. Funct. Mater. 30 (2020) 2003430.
[30] N. Wen, B. Jiang, X. Wang, Z. Shang, D. Jiang, L. Zhang, C. Sun, Z. Wu, H. Yan, C. Liu, Z. Guo, Overview of polyvinyl alcohol nanocomposite hydrogels for electro-skin, actuator, supercapacitor and fuel cell, Chem. Rec. 20 (2020) 773–792.
[31] V. Rac, S. Lević, B. Balanč, B. Olalde Graells, G. Bijelić, PVA Cryogel as model hydrogel for iontophoretic transdermal drug delivery investigations. Comparison with PAA/PVA and PAA/PVP interpenetrating networks, Colloids Surf., B 180 (2019) 441–448.
[32] J. Han, T. Lei, Q. Wu, High-water-content mouldable polyvinyl alcohol-borax hydrogels reinforced by well-dispersed cellulose nanoparticles: dynamic rheological properties and hydrogel formation mechanism, Carbohydr. Polym. 102 (2014) 306–316.
[33] F. Ji, J. Li, G. Zhang, W. Lan, R. Sun, C.-P. Wong, Alkaline monomer for mechanical enhanced and self-healing hydrogels based on dynamic borate ester bonds, Polymer 184 (2019) 121882.
[34] E. Aeridou, D. Díaz Díaz, C. Alemán, M.M. Pérez-Madrigal, Advanced functional hydrogel biomaterials based on dynamic B–O bonds and polysaccharide building blocks, Biomacromolecules 21 (2020) 3984–3996.
[35] S. Spoljaric, A. Salminen, N.D. Luong, J. Seppälä, Stable, self-healing hydrogels from nanofibrillated cellulose, poly(vinyl alcohol) and borax via reversible crosslinking, Eur. Polym. J. 56 (2014) 105–117.
[36] Y. Zhou, C. Wan, Y. Yang, H. Yang, S. Wang, Z. Dai, K. Ji, H. Jiang, X. Chen, Y. Long, Highly stretchable, elastic, and ionic conductive hydrogel for artificial soft electronics, Adv. Funct. Mater. 29 (2019) 1806220.
[37] K. Song, W. Zhu, X. Li, Z. Yu, A novel mechanical robust, self-healing and shape memory hydrogel based on PVA reinforced by cellulose nanocrystal, Mater. Lett. 260 (2020) 126884.
[38] A.F. Lourenço, J.A.F. Gamelas, T. Nunes, J. Amaral, P. Mutjé, P.J. Ferreira, Influence of TEMPO-oxidised cellulose nanofibrils on the properties of filler-containing papers, Cellulose 24 (2016) 349–362.
[39] J. Wei, Y. Chen, H. Liu, C. Du, H. Yu, Z. Zhou, Thermo-responsive and compression properties of TEMPO-oxidized cellulose nanofiber-modified PNIPAm hydrogels, Carbohydr. Polym. 147 (2016) 201–207.
[40] H. Liao, X. Guo, P. Wan, G. Yu, Conductive MXene nanocomposite organohydrogel for flexible, healable, low-temperature tolerant strain sensors, Adv. Funct. Mater. 29 (2019) 1904507.
[41] C. Shao, L. Meng, M. Wang, C. Cui, B. Wang, C.-R. Han, F. Xu, J. Yang, Mimicking dynamic adhesiveness and strain-stiffening behavior of biological tissues in tough and self-healable cellulose nanocomposite hydrogels, ACS Appl. Mater. Interfaces 11 (2019) 5885–5895.
[42] C. Li, A. Iscen, H. Sai, K. Sato, N.A. Sather, S.M. Chin, Z. Álvarez, L.C. Palmer, G. C. Schatz, S.I. Stupp, Supramolecular–covalent hybrid polymers for light-activated mechanical actuation, Nat. Mater. 19 (2020) 900–909.